



# On the performance of a tunable grating-based high sensitivity unidirectional plasmonic sensor

JAVIER GONZÁLEZ-COLSA, GUILLERMO SERRERA, JOSÉ M. SAIZ,  
FRANCISCO GONZÁLEZ, FERNANDO MORENO, AND PABLO  
ALBELLA

Group of Optics, Department of Applied Physics, University of Cantabria, 39005, Spain  
[pablo.albella@unican.es](mailto:pablo.albella@unican.es)

**Abstract:** Optical biosensing is currently an intensively active research area, with an increasing demand of highly selective, sensitivity-enhanced and low-cost devices where different plasmonic approaches have been developed. In this work we propose a tunable optimized grating-based gold metasurface that can act both as a high sensitivity sensor device (up to 1500 nm/RIU) and as an unidirectional plasmon source. The theory behind surface plasmon polariton generation is recalled to thoroughly understand the influence that every parameter of the grating source has on the performance of the proposed device. The results and conclusions discussed here offer a key step toward the design of biosensors based on excitation of surface plasmons polaritons by grating-based structures or in the process of creating new nanophotonic circuit devices.

© 2021 Optical Society of America under the terms of the [OSA Open Access Publishing Agreement](#)

## 1. Introduction

Nowadays, optical biosensors based on evanescent field analysis are highly demanded due to their simplicity, selectivity, low cost and sensitivity. Several approaches have been suggested, including holey fiber sensing [1], total internal reflection fluorescence devices [2] or Surface Plasmon Resonance (SPR) sensors [3]. However, the sensitivity of these devices is often not enough to detect low concentrations of analyte, so it is crucial to perform an accurate optimization of nanostructured systems to reach the maximum performance from these biosensors.

In particular, SPR sensors offer specific characteristics such as real time response, label-free detection and high sensitivity. The first high sensitivity label-free surface plasmon sensor was obtained in 1999 [4] and recently many SPR-based applications have been reported in areas as different as food safety [5–7], chemistry [8], medical diagnostics [9], sensing [10,11], SPR imaging (SPRi) [12] or SEIRS [13,14]. This wide range of potential applications has led researchers to explore novel ways to improve the performance of such techniques. The most popular variants of plasmonic sensors are those based on Surface Plasmon Polaritons (SPPs), which are also widely used in nanophotonic circuitry, where plasmonics offers opportunities for integrated ultrafast optoelectronic devices. SPPs, unlike SPRs that are tied to nanostructures, are electromagnetic waves coupled with surface plasma oscillations that propagate along a dielectric/metal interface. Since its prediction by Ritchie in 1957 [15], it is known that a SPP cannot be excited by just impinging light to a plane interface due to its non-radiative nature. For a SPP to be generated a coupler is needed, being the ATR (Attenuated Total Reflection) and the grating couplers among the most typically used. Plasmons are characterized by their electric field properties: the in-surface electric field component (a longitudinal wave) and the surface normal component which is an evanescent field that can act as a sensor for the dielectric medium. A change in the refractive index of the surrounding environment leads to a variation in the SPP wavevector that translates in a shift of the SPR peak wavelength position, giving rise to an accurate sensing mechanism.

In Ref. [16], Nylander et al. explored the application of ATR couplers in the area of sensing. This approach led to the development of commercial sensor systems and, due to its relative simplicity, are commonly used for characterization of thin films and biochemical sensing [17,18]. On the other hand, the use of grating-based sensors has been supported by Cullen et al. [19]. Since then, systems based on that configuration are being widely studied and optimized in order to achieve more accurate and precise sensors. The usual sensitivities obtained by some researchers range from 85 °/RIU to 800 °/RIU [20–23] using theoretical grating models or silver/gold bimetallic grating systems at angle interrogation and from 400 nm/RIU to 800 nm/RIU [24–26] in wavelength interrogation. In fact, some theoretical works [27] report on the possibility of reaching sensitivities of 1200 nm / RIU with a single material grating, achieving up to 1800 nm / RIU with more sophisticated 2D-materials grating sensors [28,29]. Extreme sensitivities up to 30000 nm/RIU have also been reported considering complex multilayer structures with hyperbolic materials [30]. A mixed approach can be considered as an alternative for ATR couplers and grating-based sensors. Starting from a simple ATR system, a diffraction grating can be added so that, due to the amount of momentum added by the grating, the coupling incidence angle for the ATR system decreases. Sensitivities of 50 °/RIU to 60 °/RIU have been obtained with these sensors [31,32].

Another important feature when considering SPP coupling is the direction of the emitted plasmon, which is known to be controllable by considering different approaches. For instance, two gratings and a single slit can generate a strong off-axis directional beaming control [33,34] or a single rectangular unit cell and two slits also allow to control the coupling between light and the SPP, enabling a directional propagation [35]. Furthermore, in [36,37] the strong directional selectivity was studied for nonsymmetric metallic gratings with double-side corrugations and variable periods. Some research groups have managed to control the coupling direction by means of complex nanostructures made of graphene, built by rotating gratings or with phase discontinuities [38–40]. However, one of the most interesting and simplest ways to control the propagation direction of plasmons would be to use only the incident polarization.

In this work, we recall the theory behind surface plasmon polariton generation to thoroughly understand the influence that every parameter of a 1D grating source has on the performance of such a device both as a controllable one-way SPP source and as a sensor. We show that a careful optimization of metasurfaces based on an easy to fabricate gold diffraction grating reduces the aforementioned limitations of typical metasurfaces [41–44]. The proposed optimization offers both, flexible and efficient control of the plasmon propagation direction, and a direct sensing tool that can significantly improve the actual sensitivities to dielectric targets. Next, we show that the behavior of this structure can be extended to a two-dimensional grating without perturbing the directional and sensing features of the device. Finally, we also demonstrate how this kind of device can be applied to enhance molecule absorption of an artificial absorbing material (pseudo-PMMA) layer.

## 2. Theory and structure model

When a TM-polarized wave with a wavelength,  $\lambda$ , impinges on a metallic grating, a SPP can be generated due to the coupling between the incident electric field and the oscillations of the free electrons in the metal surface. This coupling - noticeable by a characteristic dip in the reflection pattern - takes place when the incident radiation wavevector, assisted by the diffraction grating, is resonant with the plasmon wavevector. In other words, the following equation is satisfied

$$k_0 n \sin \theta + m \frac{2\pi}{\Lambda} = \pm k_0 \sqrt{\frac{n^2 \epsilon}{n^2 + \epsilon}} \quad (1)$$

where  $m$  is the diffraction order,  $\theta$  is the angle of incidence,  $\Lambda$  is the grating period,  $n$  the refractive index of the surrounding medium,  $k_0$  the wavevector of light in free space and  $\epsilon$  is the real part of

the dielectric constant of the metal. The order  $m$  can be positive or negative and the + and - signs refer to the propagation sense of plasmons. In general, due to the high contrast between the refractive indices of the metal and dielectric surrounding media, the square root term in Eq. (1) can be Taylor expanded, obtaining the following expression

$$n \sin \theta + |m| \frac{\lambda}{\Lambda} \approx n \left( 1 + \frac{1}{2} \delta + O(\delta^2) \right) \quad (2)$$

where  $\delta = \frac{n^2}{|\epsilon|}$  must satisfy  $\delta \ll 1$ . The surface plasmon resonance sensor designed in this work takes advantage of the strong dependence on  $n$  to detect little changes in the refractive index of the dielectric environment.

### 2.1. Refractive index sensing mechanism

One of the most important parameters that defines the performance of a grating working as a sensor is its sensitivity,  $S$ . This parameter is defined as the change in the spectral position of the reflection dip with respect to the change in the environment refractive index. When plasmons are generated at the dielectric/metal interfaces their evanescent field is influenced by the surrounding medium producing a variation in the coupling conditions and plasmons excitation wavelength. A simple expression for the grating sensitivity can be obtained from Eq. (2)

$$S = \frac{d\lambda}{dn} \approx \frac{\Lambda}{|m|} \left( 1 - \sin \theta + \frac{3}{2} \frac{n^2}{|\epsilon|} \right) \quad (3)$$

When plasmonic excitation occurs, several plasmons with different orders can be generated, resulting in different minima in the reflection spectrum. These minima have broad full width at half maximum (FWHM) making difficult their characterization. The function of merit (FOM) given by

$$FOM = \frac{S}{FWHM} \quad (4)$$

takes care of this by relating the sensitivity to  $n$  and the resolution capability associated to the SPR. Therefore, high FOM values, corresponding to prominent and narrow dips, represent more accurate devices.

Finally, the  $Q$ -factor is an indicator of the sensor quality. It can be calculated as

$$Q - factor = \frac{\lambda}{FWHM} \quad (5)$$

where  $\lambda$  is the spectral position of the reflection dip.

### 2.2. Proposed structure

In Fig. 1 we show the proposed structure. The grating properties and its ability to generate and support SPPs have been investigated using a two-dimensional finite-difference time-domain method (2D-FDTD, Lumerical software). The simulation region has been considered as a two-media (gold/dielectric) system separated by a gold diffraction grating as can be seen in the inset of Fig. 1. Perfectly matched layer (PML) absorption boundary conditions were used at all boundaries. A TM-plane wave has been considered for all 2D calculations in order to generate SPPs. The previous system has also been extended to a two-dimensional square grating as seen in Fig. 1 and has been analyzed using the three-dimensional finite-difference time-domain method (3D-FDTD).

The 2D grating is built on a gold layer thicker than the skin depth for the working spectrum so that no energy is lost through the layer. The entire structure rests on a glass substrate. Two different simulation strategies have been followed. First, to study the response of the metasurface as a tunable unidirectional SPP source, a finite system illuminated by a Gaussian beam source

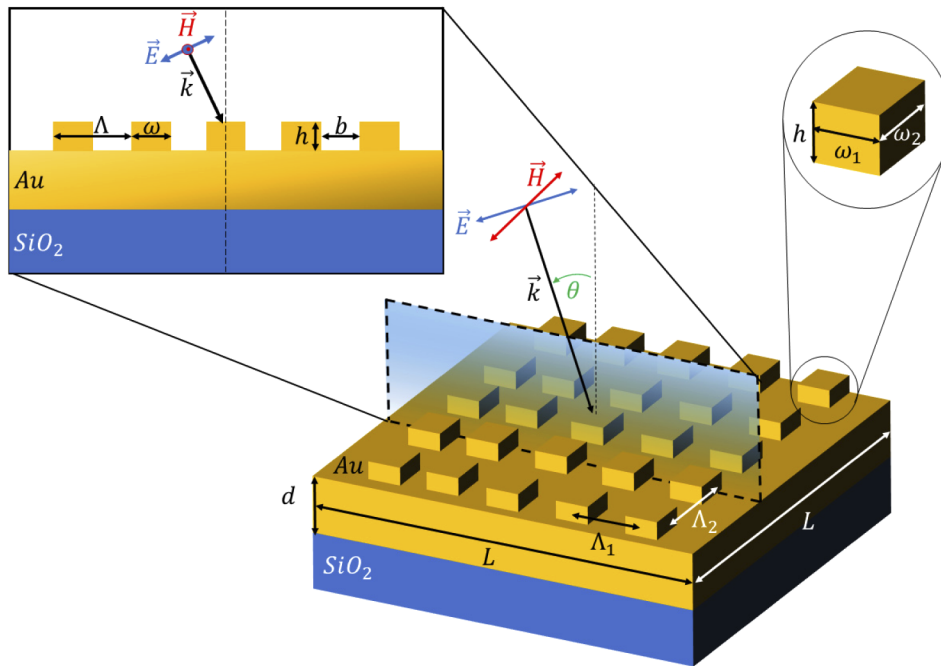


**Fig. 1.** Structure of the proposed sensor.  $\Lambda_1$  and  $\Lambda_2$  are the grating periods,  $L$  is the length of the whole system and  $d$  is the gold substrate thickness. The inset on the left shows a 2D slice where  $\Lambda$  is the grating period,  $h$  is the cell height,  $\omega$  is the cell width and  $b$  is the distance between cells. The inset on the right represents a unit cell where  $\omega_1$  and  $\omega_2$  are the cell widths and  $h$  the cell height.  $\vec{E}$ ,  $\vec{H}$  and  $\vec{k}$  are the electric and magnetic field and the wavevector respectively.  $\theta$  is the angle of incidence.

was employed to avoid numerical injection errors. And second, to estimate the sensitivity of the metasurface when acting as a sensor, a grating composed of an infinite number of unit cells illuminated by a monochromatic plane wave was considered.

### 3. Results and discussions

The initial study consists in the optimization of all grating parameters such as period, unit cell height and width in order to obtain the best plasmonic response. For a better understanding of the structure, an optimization of the 1D grating to reduce the number of variables is made. Incidence parameters (i.e. angle and polarization) were also studied together with the sensing properties and the selective behavior of the device. Furthermore, the grating has been extended to a more realistic two-dimensional system and its ability to control the plasmon propagation direction is also evidenced. Finally, the enhanced sensing response to a fictitious pseudo-PMMA molecule is investigated.

#### 3.1. Grating optimization to control the surface plasmon propagation sense

Starting with the 1D geometry shown in the inset of Fig. 1, the grating optimization began with the inspection of its integrated reflectivity for duty cycles ( $r = \frac{\omega}{\Lambda}$ ) ranging from 0.1 to 0.9. A unit cell height of  $h = 30$  nm was considered for all systems because it produces a high reflectivity drop for the smallest resonance wavelength. Figure S1 of [Supplement 1](#), shows the reflectivity of different grating heights from 30 to 70 nm, where almost no difference can be noticed. This

shows the robustness of the proposed design to possible fabrication limitations. Figure 2 shows a comparison of the reflectivity obtained as a function of the angle of incidence of two gratings for  $r = 0.5$  and  $r = 0.7$ , respectively, being the last an optimal case since both minima are perfectly split and present a high drop in reflectivity at the same time. A duty cycle of  $r = 0.8$  can be an acceptable candidate for the purpose (please see [Supplement 1](#), Fig. S2 for a full set of  $r$  cases).

Starting the analysis from the shortest wavelength, the reflectance shows low values for all incidence angles, just showing a single broad minimum (pseudo-Brewster angle) according to the Fresnel equations for gold. As the wavelength increases, gold starts to behave more as a perfect conductor, thus, the reflectance increases, and new interesting minima appear associated to the excitation of SPPs, each of them corresponding to opposite sense propagating SPPs according to Eq. (1). The different values of the minima for  $r = 0.5$  and  $0.7$  gratings are a consequence of the optimization process. As for the angle of incidence, in the case of optimal SPP coupling, it can be seen how it evolves from  $\lambda = 550$  nm (where both dips almost overlap) to  $\lambda = 650$  nm (where they are clearly separated). This occurs because the magnitude of the incident wavevector becomes smaller as the wavelength grows. To make sure that the grating receives the necessary amount of momentum, the projection of the wavevector along the generated SPP direction, must change. This is achieved by varying the angle of incidence.

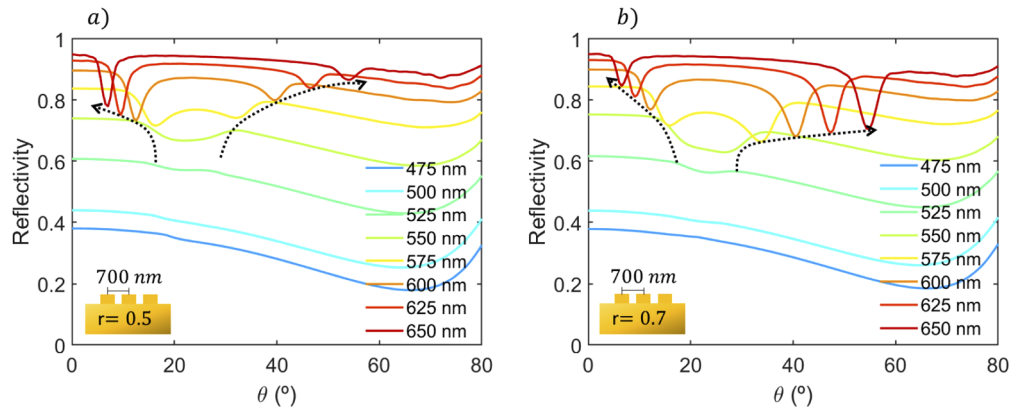


**Fig. 2.** Grating reflectivity versus angle of incidence for a set of wavelengths in the optical range. The period is 700 nm and the cell height 30 nm. The legend corresponds to the different illumination wavelengths.

According to Eq. (1), the opposite propagating SPPs correspond to different diffraction orders with opposite signs ( $m = 1$  and  $m = -2$ ). This implies that plasmons are propagating in opposite ways for the same wavelength. Thus, an adequate grating optimization allows to enhance higher diffraction order responses in such a way that propagation direction of plasmons can be controlled by changing one of the incidence parameters, either by keeping the wavelength constant and changing the incidence angle or vice versa.

For a better analysis of the SPP generation, the corresponding near field maps are shown in Fig. 3. These maps show the result of the interaction between the incident radiation and the gold grating response at each of the previously optimized minima for an incident wavelength of 600 nm. This is the smallest wavelength in our set for which both minima are perfectly split allowing to make the FDTD region smaller reducing memory requirements. As expected, the intensity distribution increases exponentially as the metal interface is approached. This can be explained according to the plasmon's evanescent decay in the dielectric medium [45].

Another remarkable aspect is the interference that appears on the upper side of the SPP that is produced due to the interaction between the incident and reflected waves. The most interesting

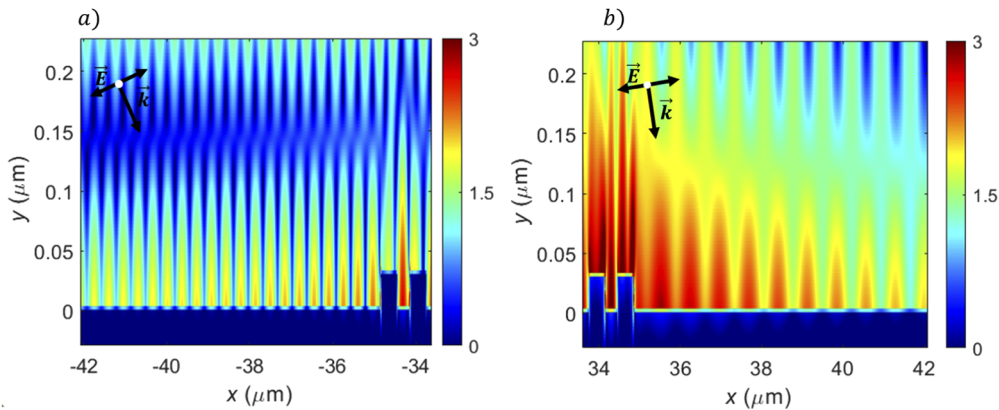


**Fig. 3.** Near field intensity maps for a gold grating with  $\Lambda = 700 \text{ nm}$ ,  $h = 30 \text{ nm}$  and  $r = 0.7$ .  
(a) Left-side of the grating for  $\theta = 39.49^\circ$ . (b) Right-side of the grating for  $\theta = 13.17^\circ$ .  $\vec{E}$ ,  $\vec{H}$  and  $\vec{k}$  are the electric and magnetic fields and the wavevector of the incident radiation.

feature in Fig. 3 is that both plasmons, the second order plasmon going to the left and the first order plasmon going to the right, have different wavelengths, intensity and propagation distances according to their different wavevectors.

### 3.2. Grating-based sensor design

In order to analyze the performance of the proposed platform as a refractive index sensor of arbitrary dielectric surrounding media, the sensitivity is calculated for periods in the range  $\Lambda = [700, 1500] \text{ nm}$  by simulating the reflectivity as a function of the excitation wavelength for a range of refractive indices [1.32-1.34]. The strategy followed here consisted in looking for variations in the sensitivity upon changes in the grating parameters so that plasmon generation was still allowed. Equation (3) shows that sensitivity increases with the period and decreases with the incidence angle. Thus, in order to increase the sensitivity, we must increase the grating period  $\Lambda$ . Normal incidence was assumed here because it offers maximum sensitivity and compactness for each case.

Figure 4 compares the theoretical sensitivity obtained by Eq. (3) with the simulated sensitivities, considering also the estimated error that accounts for higher order terms in the Taylor expansion. In general, all cases agree well with the theoretical model and the error decreases when sensitivity increases, thus, the model will be more accurate in the most sensitive systems. Figure 4 also shows that more sensitive gratings must be excited with larger wavelengths according to Eq. (2). Since the grating is built on gold, the real and imaginary parts (Johnson & Christy [46]) of the dielectric constant also grow. This results in larger resistive losses, therefore reducing the plasmon efficiency. For this reason, systems with periods larger than 1500 nm show poorly-defined dips, hindering the performance of the sensor and allowing to obtain the best sensitivity (1500 nm/RIU).

The quality properties - dip FWHM, the figure of merit (Eq. (4)) and the quality factor (Eq. (5)) - of this best result, shown in Fig. 5, are calculated as a function of the duty cycle  $r$  ranging from 0.1–0.9 for an optimal grating with 150 periods. The wavelength of the reflection minima grows first and then decreases as the duty cycle increases (see Fig. 5(a)). This can be explained by considering the unit cell length. When that length grows, electrons are free to move in a larger path, resulting in a red-shift in the minimum. However, the distance between unit cells is reduced in the process inducing a blue-shift for duty cycles greater than 0.7. The different reflection minima are the result of the optimization process. Considering the different quality

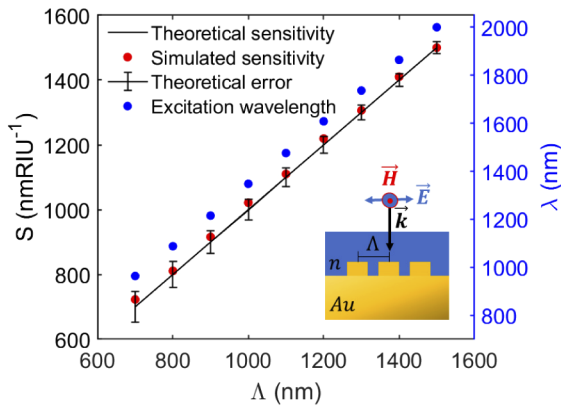


**Fig. 4.** Sensitivity of the proposed sensor with respect to the grating period. The theoretical sensitivity from Eq. (3) (black line) is shown along with the simulated sensitivity (red dots) and the theoretical error (error bars). The wavelength excitation of the system is also shown (blue dots).

factors shown in Fig. 5(b)–(d) the best performance of the sensor has been obtained at duty cycle of  $r = 0.3$  with a figure of merit of 161.46, a Q-factor of 214.69 and a FWHM of 9.29 nm.

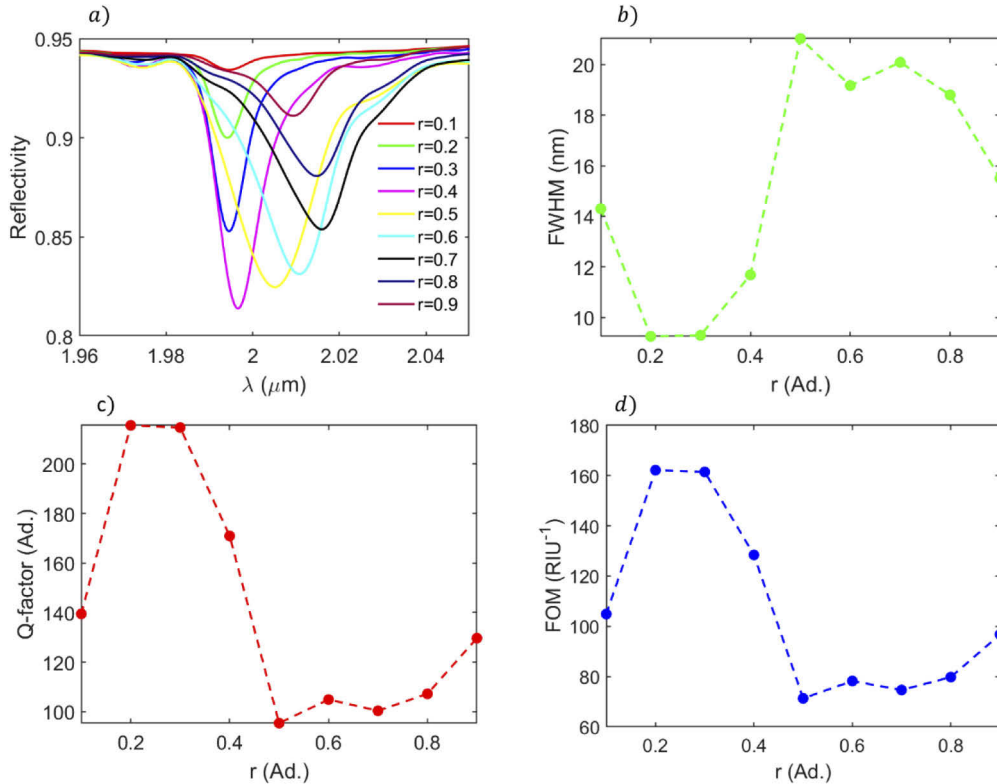


**Fig. 5.** (a) Grating reflectivity as a function of wavelength for a set of duty cycles. (b) Full width at half maximum for the minima in (a) with respect to the duty cycle. (c) Quality factor for the minima in (a). (d) Figure of merit for the minima in (a).

### 3.3. Two-dimensional grating system: directionality

A straightforward attempt to extend the selective 1D directional SPP generator geometry to a 2D one would be considering a grating of long enough ribs in such a way that the 2D and 3D calculations would be formally equivalent. Such a system would only allow plasmon propagation control in one direction. However, the grating exposed in Fig. 1 suggests that it is possible to control the plasmon propagation in the two main plane directions once carefully optimized. To visualize how this structure works, the directionality and sensitivity for a symmetrical case is shown, with  $\Lambda_1 = \Lambda_2 = 700$  nm, widths  $\omega_1 = \omega_2 = 490$  nm, blanks  $b_1 = b_2 = 210$  nm and  $h = 30$  nm, which are the previously optimized 1D system features. The ability of the 2D grating to direct plasmons is exposed in a set of near field maps trying to mimic the SPP generation conditions of the 1D system. Due to the finite dimensions of this case (10 periods), PML boundary conditions around the entire system have been considered, while a broad Gaussian beam has been used to avoid numerical injection errors.

Figure 6 shows the result of the interaction between the linearly polarized Gaussian beam and the grating at normal incidence. In Fig. 6(a) the incident polarization is parallel to  $x$ -axis and in Fig. 6(b) is parallel to  $y$ -axis. In both cases symmetric SPPs are generated, each one travelling parallel to the incident polarization direction but in opposite senses. The background field corresponds to the residual electric field of the Gaussian beam. This demonstrates that the propagation direction of plasmons can be controlled by simply changing the incident polarization. One step further consists in exploring a way to control the SPP propagation sense, coinciding with the incident polarization of light. This, according to Eq. (1), requires the excitation of opposite sign modes. Recalling Fig. 2, this can only be done by changing the excitation angle, i.e. using oblique incidence, since the different modes are associated with the wavevector projection along the polarization axis. Changing the incidence angle also modifies that projection, thus allowing the excitation of different sense modes.

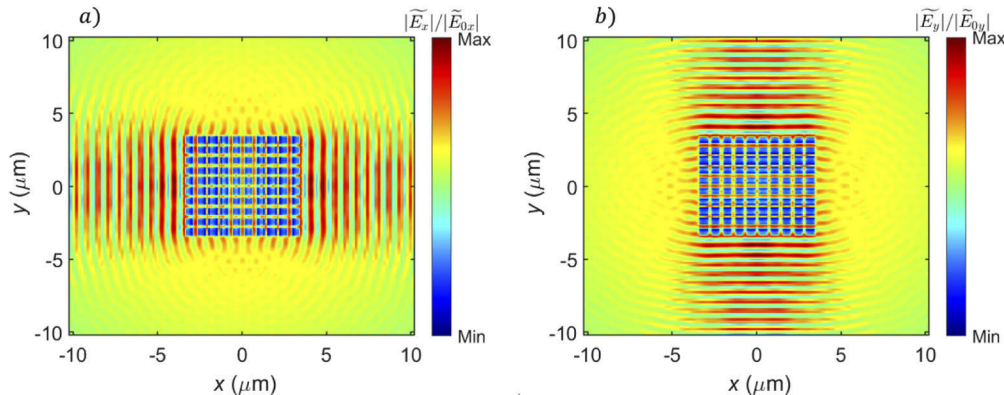


**Fig. 6.** Grating near field maps at normal incidence. (a) corresponds to an  $x$ -polarized incident wave and (b) to an  $y$ -polarized incident wave (for more details see [Visualization 1](#) and [Visualization 2](#)).

To illustrate this effect, Fig. 7(a)–(d) shows a set of near field maps corresponding to SPPs travelling along  $-x$ ,  $+x$ ,  $-y$  and  $+y$ , respectively (please, see the Visualizations in the supplementary information for an illustrative view of this effect). As these SPPs correspond to oblique incidence excitation, the incident electric field in-plane component makes difficult to distinguish the unidirectional travelling plasmon. To remove that contribution, the SPP electric field is normalized to the respective incident electric field component leaving only the most intense propagating mode. Additionally, a weak propagating wave along the orthogonal direction

to the plasmon propagation is shown. This background is a consequence of the interactions between different arrays of unit cells resulting in higher order modes excitation. We can conclude that the SPP propagation sense can be controlled by changing the polarization and the incidence angle. Therefore, the proposed 2D system generalizes the 1D system previously studied and allows more control over the direction of the generated plasmons, with the grating acting as a sensor element.

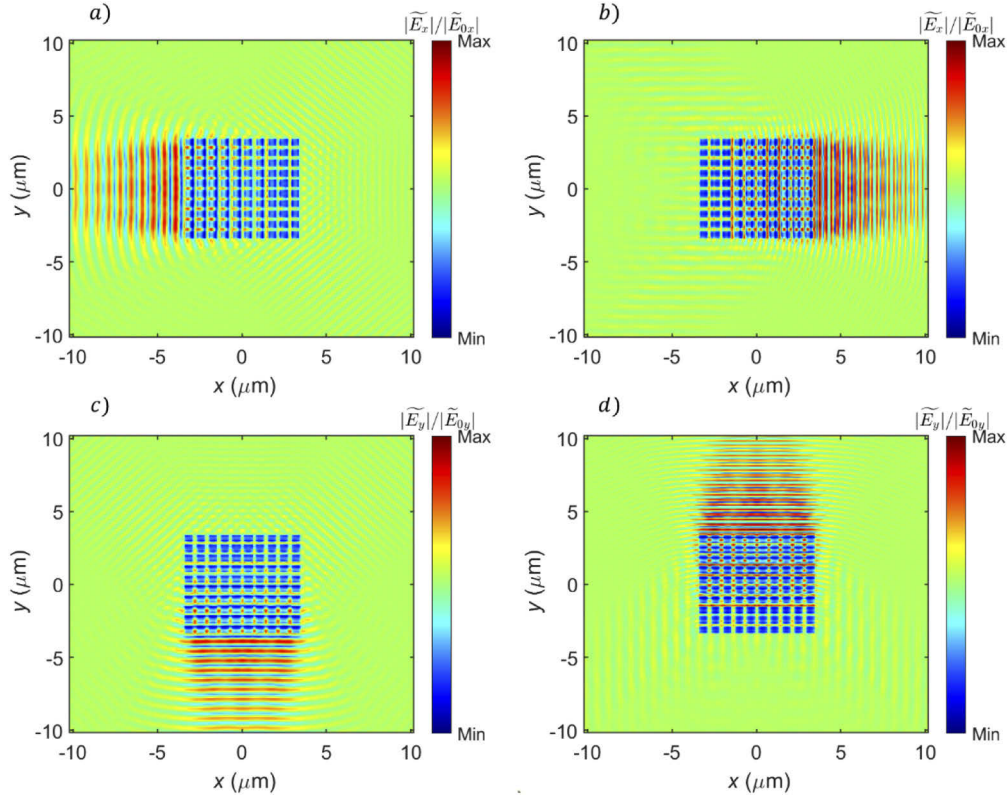


**Fig. 7.** Grating near field maps at oblique incidence. (a) corresponds to an x-polarized incident wave and  $\theta = 13.17^\circ$  (b) to an x-polarized incident wave and  $\theta = 39.49^\circ$ , (c) to a y-polarized incident wave and  $\theta = 13.17^\circ$  and (d) to a y-polarized incident wave and  $\theta = 39.49^\circ$ . Angles of incidence are considered positive in all cases (for more details see [Visualization 3](#), [Visualization 4](#), [Visualization 5](#) and [Visualization 6](#)).

### 3.4. Two-dimensional grating system: molecule sensing

Once the directionality in the 2D design is shown, we investigate the response of our system to the presence of different coatings of aqueous target samples. To do that, the reflectivity spectrum of the entire system has been calculated with the structure surrounded by a dielectric medium of refractive index ranging from 1.32 to 1.34. Figure 8 shows the reflective minima obtained for a grating. The minima are red-shifted when the environment refractive index grows. This happens because as the refractive index increases the wavelength of the plane wave are compressed and therefore the corresponding emission wavelength must grow. By taking the wavelength displacement with respect to the refractive index change, sensitivity can be calculated. The obtained sensitivity  $S = 728 \text{ nm/RIU}$ , is in perfect agreement with the 1D model results. This implies that the 1D theoretical sensitivity can also be achieved in this 2D grating. Now, we

can combine this high sensitivity with the other interesting ability of the proposed platform, the selective directional SPP generation.

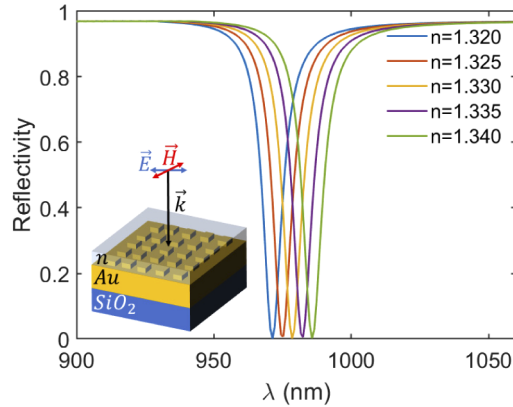


**Fig. 8.** Grating reflectivity as a function of wavelength in vacuum for a changing dielectric environment refractive index.

Following the same strategy as in Ref. [14], the performance of the proposed sensor has been tested in a more realistic situation. A 10 nm-thick layer of an artificial absorbing material (pseudo-PMMA) has been considered as a sample. The theoretical permittivity of this material follows an ideal single frequency Lorentz model and presents an absorption peak near a wavelength of 800 nm as shown in the inset of Fig. 9(a). When the pseudo-PMMA sample is on top of a gold substrate without the grating sensor, the reflectivity shows a very weak decrease around 800 nm due to the pseudo-PMMA absorption (see upper inset). The blue curve corresponds to the reflectivity of an infinite gold grating of period  $\Lambda = 700$  nm. It can be seen an abrupt drop at the SPP wavelength.

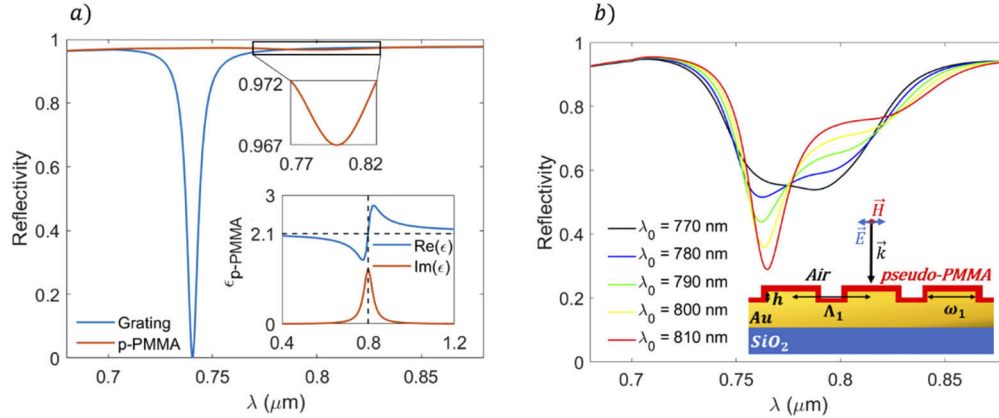


**Fig. 9.** (a) Reflectivity of a gold grating and a pseudo-PMMA layer with a resonance centered at  $\lambda_0 = 800$  nm without grating. The PMMA permittivity is shown in the inset with a real part base line of = 2.1. (b) Reflectivity of the structures shown in the inset composed by a gold grating covered with a 10 nm pseudo-PMMA layer for different theoretical resonances positions  $\lambda_0$ .

When the pseudo-PMMA layer of molecules is deposited on the grating sensor, its absorption is significantly enhanced. This effect increases as the SPP resonance gets closer to the pseudo-PMMA absorption wavelength. This enhancement can be verified by redesigning the grating geometry or by shifting the absorption of the artificial molecule. For simplicity, we consider the second option, i.e. shifting its theoretical absorption wavelength  $\lambda_0$  from 770 to 810 nm and calculating the grating reflectivity for each case. These results are shown in Fig. 9(b), where two local minima appear, being the SPR one the most noticeable. In general, the SPR wavelength is now red-shifted. When a pseudo-PMMA layer is considered, the SPR is influenced by the base line of the surrounding refractive index and consequently in a redshift according to Eq. (1). When the pseudo-PMMA resonance is tuned to the SPR, its absorption is significantly enhanced and consequently a shallower plasmon deep can be seen. Both minima reach the same depth at  $\lambda_0 = 770$  nm approximately so that the pseudo-molecule absorption can be clearly detected and analyzed.

#### 4. Conclusions

A theoretical analysis of the sensitivity of a regular grating-based metasurface shows that the optimization of the unit cell geometrical parameters and its duty cycle produces more sensitive tunable devices, reaching a maximum sensitivity of 1500 nm/RIU by fixing the normal incidence for an aqueous media in the near infrared. Moreover, we have shown that this metasurface can work as a directional coupler, and that depending on the polarization and the angle of incidence, the SPP direction and propagation sense can be efficiently controlled.

Finally, we have tested the sensing performance of the metasurface by analyzing the absorption of an ideal single resonance Lorentz modelled molecule located on the proposed grating showing how it can be strongly enhanced by coupling the SPP resonance and the molecule absorption. The results and conclusions of this work can be very interesting and useful to improve the quality of state-of-the-art biosensors or to designing new grating-based high sensitivity devices. Our results can also assist experimentalists to develop robust and helpful nanometric optoelectronic components that accelerate the development of integrated optical circuits. Although, gold is the plasmonic material often used due to its biological compatibility and chemical stability, our optimization guide can be extended to other spectral regimes by just reconfiguring the geometrical parameters and choosing the appropriate plasmonic material (i.e. the necessary optical properties to satisfy the dispersion relation at the desired frequency).

**Funding.** Ministerio de Economía, Industria y Competitividad, Gobierno de España (PGC2018-096649-B-I).

**Acknowledgments.** We gratefully acknowledge financial support from Spanish national project INMUNOTERMO (No. PGC2018-096649-B-I). J. G-C. thanks the Ministry of Science of Spain for his FPI grant. G. S. thanks the Ministry of Education for his collaboration grant and P.A. acknowledges funding for a Ramon y Cajal Fellowship (Grant No. RYC-2016-20831).

**Disclosures.** The authors declare no conflict of interest.

**Supplemental document.** See [Supplement 1](#) for supporting content.

#### References

1. A. S. Webb, F. Poletti, D. J. Richardson, and J. K. Sahu, "Suspended-core holey fiber for evanescent-field sensing," *Opt. Eng.* **46**(1), 010503 (2007).
2. D. Axelrod, T. P. Burghardt, and N. L. Thompson, "Total Internal reflection fluorescence," *Annu. Rev. Biophys. Bioeng.* **13**(1), 247–268 (1984).
3. C. M. Miyazaki, F. M. Shimizu, and M. Ferreira, "Surface Plasmon Resonance (SPR) for Sensors and Biosensors", in *Nanocharacterization Techniques* (William Andrew, 2017).
4. J. Homola, I. Koudela, and S. S. Yee, "Surface plasmon resonance sensors based on diffraction gratings and prism couplers: sensitivity comparison," *Sens. Actuators, B* **54**(1-2), 3–15 (1999).
5. Z. Samavati, A. Samavati, A. F. Ismail, M. A. Rahman, and M. H. D. Othman, "Detection of saline-based refractive index changes via bilayer ZnO/Ag-coated glass optical fiber sensor," *Appl. Phys. B: Lasers Opt.* **125**(9), 161 (2019).
6. Z. Altintas, "Surface plasmon resonance based sensor for the detection of glycopeptide antibiotics in milk using rationally designed nanoMIPs," *Sci. Rep.* **8**(1), 11222–12 (2018).

7. B. J. Yakes, J. Deeds, K. White, and S. L. DeGrasse, "Evaluation of surface plasmon resonance biosensors for detection of tetrodotoxin in food matrices and comparison to analytical methods," *J. Agric. Food Chem.* **59**(3), 839–846 (2011).
8. T. Arakawa, H. Yasukawa, and K. Fujimoto, "Detection of alcohol vapor using surface plasmon resonance sensor with organic-inorganic hybrid layers," *Sensors Mater.* **22**(4), 201–209 (2010).
9. P. K. Teotia and R. S. Kaler, "1-D grating based SPR biosensor for the detection of lung cancer biomarkers using Vroman effect," *Opt. Commun.* **406**(2), 188–191 (2018).
10. K. Lin, Y. Lu, J. Chen, R. Zheng, P. Wang, and H. Ming, "Surface plasmon resonance hydrogen sensor based on metallic grating with high sensitivity," *Opt. Express* **16**(23), 18599 (2008).
11. K. E. Chong, H. W. Orton, I. Staude, M. Decker, A. E. Miroshnichenko, I. Brener, Y. S. Kivshar, and D. N. Neshev, "Refractive index sensing with Fano resonances in silicon oligomers," *Philos. Trans. R. Soc., A* **375**(2090), 20160070 (2017).
12. Y. Chen, J. Liu, Z. Yang, J. S. Wilkinson, and X. Zhou, "Optical biosensors based on refractometric sensing schemes: A review," *Biosens. Bioelectron.* **144**(1), 111693 (2019).
13. P. Albellal, F. Neubrech, D. Weber, and G. Han, "Nanoantennas for surface enhanced infrared spectroscopy: Effects of interaction and higher order resonant excitations," *AAPP Atti della Accad. Peloritana dei Pericolanti Cl. di Sci. Fis. Mat. e Nat.* **89**(1), 2–5 (2011).
14. P. Alonso-González, P. Albellal, F. Neubrech, C. Huck, J. Chen, F. Golmar, F. Casanova, L. E. Hueso, A. Pucci, J. Aizpurua, and R. Hillenbrand, "Experimental verification of the spectral shift between near- and far-field peak intensities of plasmonic infrared nanoantennas," *Phys. Rev. Lett.* **110**(20), 203902 (2013).
15. R. H. Ritchie, E. T. Arakawa, J. J. Cowan, and R. N. Hamm, "Surface-plasmon resonance effect in grating diffraction," *Phys. Rev. Lett.* **21**(22), 1530–1533 (1968).
16. C. Nylander, B. Liedberg, and T. Lind, "Gas detection by means of surface plasmon resonance," *Sens. Actuators* **3**(1), 79–88 (1982).
17. C. Striebel, A. Brecht, and G. Gauglitz, "Characterization of biomembranes by spectral ellipsometry, surface plasmon resonance and interferometry with regard to biosensor application," *Biosens. Bioelectron.* **9**(2), 139–146 (1994).
18. K. A. Peterlinz and R. Georgiadis, "Two-color approach for determination of thickness and dielectric constant of thin films using surface plasmon resonance spectroscopy," *Opt. Commun.* **130**(4–6), 260–266 (1996).
19. D. C. Cullen, R. G. W. Brown, and C. R. Lowe, "Detection of immuno-complex formation via surface plasmon resonance on gold-coated diffraction gratings," *Biosensors* **3**(4), 211–225 (1987).
20. S. Nazem, M. Malekmohammad, and M. Soltanolkotabi, "Theoretical and experimental study of a surface plasmon sensor based on Ag-MgF<sub>2</sub> grating coupler," *Appl. Phys. B: Lasers Opt.* **126**(5), 96 (2020).
21. Y. Dai, H. Xu, H. Wang, Y. Lu, and P. Wang, "Experimental demonstration of high sensitivity for silver rectangular grating-coupled surface plasmon resonance (SPR) sensing," *Opt. Commun.* **416**(1), 66–70 (2018).
22. A. Bijalwan and V. Rastogi, "Sensitivity enhancement of a conventional gold grating assisted surface plasmon resonance sensor by using a bimetallic configuration," *Appl. Opt.* **56**(35), 9606–9612 (2017).
23. F. Romanato, K. H. Lee, H. K. Kang, G. Ruffato, and C. C. Wong, "Sensitivity enhancement in grating coupled surface plasmon resonance by azimuthal control," *Opt. Express* **17**(14), 12145–12154 (2009).
24. K. H. Yoon, M. L. Shuler, and S. J. Kim, "Design optimization of nano-grating surface plasmon resonance sensors," *Opt. Express* **14**(11), 4842–4849 (2006).
25. T. Iqbal and S. Afsheen, "One Dimensional Plasmonic Grating: High Sensitive Biosensor," *Plasmonics* **12**(1), 19–25 (2017).
26. A. Elrashidi, "Highly sensitive silicon nitride biomedical sensor using plasmonic grating and ZnO layer," *Mater. Res. Express* **7**(7), 075001 (2020).
27. J. Cao, Y. Sun, Y. Kong, and W. Qian, "The sensitivity of grating-based SPR sensors with wavelength interrogation," *Sensors* **19**(2), 405 (2019).
28. Z. Sadeghi and H. Shirkanli, "Highly sensitive mid-infrared SPR biosensor for a wide range of biomolecules and biological cells based on graphene-gold grating," *Phys. E (Amsterdam, Neth.)* **119**(1), 114005 (2020).
29. Y. Xu, L. Wu, and L. K. Ång, "MoS<sub>2</sub>-based Highly Sensitive Near-infrared Surface Plasmon Resonance Refractive index Sensor," *IEEE J. Sel. Top. Quantum Electron.* **25**(2), 1–7 (2019).
30. K. V. Sreekanth, Y. Alapan, M. ElKabbash, E. Ilker, M. Hinczewski, U. A. Gurkan, A. De Luca, and G. Strangi, "Extreme sensitivity biosensing platform based on hyperbolic metamaterials," *Nat. Mater.* **15**(6), 621–627 (2016).
31. C. J. Alleyne, A. G. Kirk, R. C. McPhedran, N.-A. P. Nicorovici, and D. Maystre, "Enhanced SPR sensitivity using periodic metallic structures," *Opt. Express* **15**(13), 8163–8169 (2007).
32. K. M. Byun, S. J. Kim, and D. Kim, "Grating-coupled transmission-type surface plasmon resonance sensors based on dielectric and metallic gratings," *Appl. Opt.* **46**(23), 5703–5708 (2007).
33. S. Kim, H. Kim, Y. Lim, and B. Lee, "Off-axis directional beaming of optical field diffracted by a single subwavelength metal slit with asymmetric dielectric surface gratings," *Appl. Phys. Lett.* **90**(5), 051113 (2007).
34. H. Kim, J. Park, and B. Lee, "Tunable directional beaming from subwavelength metal slits with metal–dielectric composite surface gratings," *Opt. Lett.* **34**(17), 2569–2571 (2009).
35. Y. Sonnefraud, S. Kerman, G. Di Martino, D. Y. Lei, and S. A. Maier, "Directional excitation of surface plasmon polaritons via nanoslits under varied incidence observed using leakage radiation microscopy," *Opt. Express* **20**(5), 4893–4902 (2012).

36. S. Cakmakyan, H. Caglayan, A. E. Serebryannikov, and E. Ozbay, "Experimental validation of strong directional selectivity in nonsymmetric metallic gratings with a subwavelength slit," *Appl. Phys. Lett.* **98**(5), 051103 (2011).
37. A. Pors, M. G. Nielsen, T. Bernardin, J. C. Weeber, and S. I. Bozhevolnyi, "Efficient unidirectional polarization-controlled excitation of surface plasmon polaritons," *Light: Sci. Appl.* **3**(8), e197 (2014).
38. F. Liu, C. Qian, and Y. D. Chong, "Directional excitation of graphene surface plasmons," *Opt. Express* **23**(3), 2383–2391 (2015).
39. L. Huang, X. Chen, B. Bai, Q. Tan, G. Jin, T. Zentgraf, and S. Zhang, "Helicity dependent directional surface plasmon polariton excitation using a metasurface with interfacial phase discontinuity," *Light: Sci. Appl.* **2**(3), e70 (2013).
40. J. Lin, J. P. B. Mueller, Q. Wang, G. Yuan, N. Antoniou, X.-C. Yuan, and F. Capasso, "Polarization-controlled tunable directional coupling of surface plasmon polaritons," *Science* **340**(6130), 331–334 (2013).
41. H. Chen, L. Qin, Y. Chen, P. Jia, F. Gao, C. Chen, L. Liang, X. Zhang, H. Lou, Y. Ning, and L. Wang, "Refined grating fabrication using Displacement Talbot Lithography," *Microelectron. Eng.* **189**, 74–77 (2018).
42. E. Baquedano, M. U. González, R. Paniagua-Domínguez, J. A. Sánchez-Gil, and P. A. Postigo, "Low-cost and large-size nanoplasmonic sensor based on Fano resonances with fast response and high sensitivity," *Opt. Express* **25**(14), 15967–15976 (2017).
43. K. L. Lee, T. Y. Wu, H. Y. Hsu, S. Y. Yang, and P. K. Wei, "Low-cost and rapid fabrication of metallic nanostructures for sensitive biosensors using hot-embossing and dielectric-heating nanoimprint methods," *Sensors* **17**(7), 1548 (2017).
44. H. Wang, B. Yu, S. Jiang, C. Chen, and L. Qian, "Simple and low-cost nanofabrication process of nanoimprint templates for high-quality master gratings: Friction-induced selective etching," *Appl. Surf. Sci.* **454**, 23–29 (2018).
45. H. Raether, *Surface Plasmons on Smooth and Rough Surfaces and on Gratings* (Springer, 1988).
46. P. B. Johnson and R. W. Christy, "Optical Constant of the Nobel Metals," *Phys. Rev. B* **6**(12), 4370–4379 (1972).